arXiv:1409.1922v2 [cond-mat.supr-con] 13 Jul 2015

Mechanism of metallization and superconductivity suppression in $YBa_2(Cu_{0.97}Zn_{0.03})_3O_{6.92}$ revealed by ^{67}Zn NQR

D. Pelc, M. Požek, V. Despoja, and D. K. Sunko[1]

Department of Physics, Faculty of Science, University of Zagreb, Bijenička cesta 32, HR-10000 Zagreb, Croatia.

E-mail: [1]dks@phy.hr

PACS numbers:

Abstract.

We measure the nuclear quadrupole resonance (NQR) signal on the Zn site in nearly optimally doped $YBa_2Cu_3O_{6.92}$, when Cu is substituted by 3% of isotopically pure ^{67}Zn. We observe that Zn creates large insulating islands, confirming two earlier conjectures: that doping provokes an orbital transition in the CuO_2 plane, which is locally reversed by Zn substitution, and that the islands are antiferromagnetic. Also, we find that the Zn impurity locally induces a breaking of the D_4 symmetry. Cluster and DFT calculations show that the D_4 symmetry breaking is due to the same partial lifting of degeneracy of the nearest-neighbor oxygen sites as in the LTT transition in $La_{2-x}Ba_xCuO_4$, similarly well-known to strongly suppress superconductivity. These results show that in-plane oxygen $2p^5$ orbital configurations are principally involved in the metallicity and superconductivity of all high-T_c cuprates, and provide a qualitative symmetry-based constraint on the SC mechanism.

1. Introduction

High-temperature superconductivity (SC) in the cuprate perovskites is still unexplained. They are ionic crystals with a considerable variation in composition and structure, which metallize and eventually superconduct upon doping. Their complexity makes it difficult to find properties which are universally significant for the SC mechanism. Perhaps the most important and ubiquitous structural feature of the cuprates are copper-oxide (CuO_2) planes, where metallization occurs. Yet the wave functions of the superconducting charge carriers in the planes remain enigmatic, and have been the object of intense speculation. The doping mechanism — how impurities introduce these carriers into the CuO_2 planes in the first place — has received comparatively much less attention. Our aim in this work is to gain microscopic information on both the doping mechanism and the orbital composition of the SC carriers by varying their chemical environment, substituting a small amount of in-plane copper with zinc.

Two effects lower the SC temperature T_c in cuprates so abruptly that they may be interfering with the SC mechanism itself. One is the low-temperature orthorombic-to-tetragonal (LTO/LTT) transition in $La_{15/8}Ba_{1/8}CuO_4$ (LBCO) [1], the other is

Zn substitution of the in-plane coppers. While the former appears only in the La cuprates, the Zn effect is observed in all of them. NMR has found [2] that the Curie response appearing in underdoped $YBa_2Cu_3O_{7-\delta}$ (YBCO) upon Zn substitution is due to the nearest-neighbor (nn) Cu sites, showing them to be electronically different than the bulk in-plane coppers (which carry no local spin in the SC compositions [3]). ARPES has established [4] that Zn substitution introduces no carriers into the planes, while STM has shown large screening oscillations around the Zn site, dubbed "desert islands" [5].

Upon its discovery, the Zn effect was argued [6] to provide a major insight into the SC orbital environment. The insulating undoped cuprates are antiferromagnetic (AF) insulators, with coppers in magnetic Cu^{2+} ($3d^9$) configurations, surrounded by closed-shell O^{2-} ($2p^6$) configurations. A SC-enabling orbital transition from Cu^{2+}/O^{2-} to Cu^{+}/O^{-} was conjectured [7] to occur around 6% hole doping, amounting to the donation of a hole from a copper to two oxygens. This would close the Cu $3d$ shell to $3d^{10}$, and open the O $2p$ shells to $2p^{5.5}$, implying an oxygen-dominated SC metal. The suggested driving mechanism for the orbital transition was ionic (Madelung energy change), wherein the dopands affect the crystal field without their own charges being delocalized. This scenario is henceforth referred to as *ionic doping*. Early circumstantial evidence for the orbital transition/ionic doping was the observation of the Cu^{+}/O^{-} configuration in the SC compositions using X-ray absorption spectroscopy [8]. More generally, it was found [9] that including the oxygens — explicitly via the Emery model [10], or implicitly via a second-neighbor (t') parameter [11] in the t–J model [12] — is necessary to interpret ARPES and neutron-scattering data. Significantly, this remains true also in electron-doped cuprates [13], indicating a universal feature of cuprate SC.

Alternative CuO_2 plane doping mechanisms have been contested on either theoretical or experimental grounds. The metallic alloying scenario, wherein the planes are doped with delocalized dopand holes, is contradicted by ab initio calculations showing that the Sr hole in $La_{2-x}Sr_xCuO_4$ remains localized [14]. It is similarly found that the interstitial oxygen in $La_2CuO_{4+\delta}$ preferentially creates an inert peroxide, O_2^{2-}, with the apical oxygen [15]. A more remote possibility, the impurity-band scenario, is excluded experimentally [16]. Thus the original ionic doping idea [7, 17] was left uncontested by default, yet without microscopic experimental corroboration. Zn substitution of in-plane Cu provides a unique opportunity to test it: because Zn^{2+} already has a closed $3d$ shell, it has no hole to donate to the neighbouring oxygens. It should then revert them to the parent $2p^6$ and thus locally undo the orbital transition [6]. Such local reversal implies a characteristic signature — Coulomb "domino effect" of charge redistribution around the Zn site — because the charge mismatch between the O^{2-} configurations near Zn and O^{-} in the bulk was not expected to be stabilized across a single Cu site [6, 7]. In the present work, we provide direct evidence of the conjectured orbital transition and charge redistribution by measuring the nuclear quadrupole resonance (NQR) signal on the Zn site itself for the first time.

The article is organized as follows. After a summary of the methods employed in Sect. 2, we present the measurements in Sect. 3. We find that Zn creates a large insulating cluster, extending at least as far as the nn coppers, even in nearly optimally doped YBCO, and that it breaks the D_4 (square) symmetry of the planar unit cell. These observations are subject to a detailed analysis in Sect. 4, which includes extensive theoretical modelling and comparison with the results of other work,

including Cu NMR in Zn-substituted cuprates, scanning tunneling microscopy (STM), and neutron scattering. Finally Sect. 5 collects our conclusions.

2. Methods

2.1. Samples and instrumentation

Fine (micron-sized) powder samples of nearly optimally doped YBCO were prepared for the NQR experiments by a standard solid state synthesis with repeated annealing. High-purity precursor materials were used (Y_2O_3, CuO and BaO, 99.99% from Sigma-Aldrich), and the zinc was introduced by substituting 3% molar of CuO with ZnO (89.6% ^{67}Zn enriched, from Eurisotop). Samples were characterized by powder X-ray, iodometry (to determine the amount of oxygen) and Meissner shielding measurements, to confirm their phase purity and homogeneity. Meissner shielding shows a superconducting transition at 57 K with a width of $\sim$ 2 K, which is rather sharp for Zn-substituted YBCO [18, 19]. The most sensitive indication of the microscopic homogeneity of the samples is the small width of the ^{67}Zn NQR lines (shown below). Relatively large amounts of powder were used for Zn NQR due to the small concentration of zinc in the sample and low NQR frequencies, typically $\sim$ 500 mg for each sample.

Optimally doped YBCO powders were prepared with nominally 3% substitution of Cu by the isotopically purified ^{67}Zn, leading to about 4% Cu substitution in the planes, because Zn preferentially substitutes the in-plane Cu upon annealing [18, 19, 20]. Zn and Cu NQR experiments were performed with a standard spin-echo sequence, using a Tecmag Apollo NMR/NQR spectrometer and a flowing gas cryostat for sample temperature variation. In spin-lattice relaxation measurements we employed a saturation recovery sequence (with spin echo detection). Long data acquisition times, up to two weeks for observation of forbidden transitions, required special precautions to stabilize the temperature.

2.2. Cluster DFT calculations.

As the primary purpose of the cluster calculation was to explore the electronic neighbourhood of the Zn substituent and its effects on the lattice semi-quantitatively, the investigated cluster was relatively small (Fig. 4a). In addition to the atoms shown, point charges were placed on the positions of the nearest Ba and Y ions. For all calculations we used the hybrid functional B3LYP and the rather simple polarized Ahlrichs basis set [21]. The RI approximation was used throughout [22]. The employed spin multiplicity of 5 corresponded to the copper atoms being quite strongly polarized, as in previous calculations [23]. In atomic relaxation calculations the furthermost in-plane and all apical oxygen atoms, and all point charges were held fixed, with other atoms free to move. Such a procedure yielded relatively large lattice deformations, which would probably be smaller in a more realistic cluster. However, the gross symmetry features of the deformation are robust with respect to calculation parameters. Due to the computational cost of high-precision calculations, we did not undertake a quantitative comparison with the observed NQR parameters, but this should in principle be possible. We checked that the weak orthorhombicity inherent in YBCO does not change the nature of the lattice deformation brought upon by Zn substitution, compared to a perfectly tetragonal initial setting.

2.3. Supercell DFT calculations.

For the ground state electronic structure calculation we used plane-wave self-consistent field DFT code (PWscf), within the Quantum Espresso (QE) package [24], and Perdew-Burke-Ernzerhof (PBE) parametrization of the generalized gradient approximation (GGA) for the exchange-correlation potential [25]. The ground-state electronic density was calculated using a $5 \times 5 \times 1$ Monkhorst-Pack special K-point mesh, with 6 special points in the irreducible Brillouin zone. In the PWscf code we used projector-augmented-wave-based pseudopotentials for La, Cu and O atoms, and we found the energy spectrum to be convergent with a 75 Ry plane-wave cutoff. For the in-plane (1×1) unit cell parameter we used $a = 7.15696$ *a.u.* which is the experimental lattice constant commonly used in the literature. For the unit supercell in the perpendicular direction (separation between periodically repeated La_2CuO_4 planes) we artificially expand the layer spacing to $L = 3.5a = 25.11$ *a.u.*, which decreases the c-axis overlap so much that the calculation refers to a single-layer slab, appropriate for an STM simulation. The local density of states (LDOS) $\rho(E, \mathbf{r}) = \sum_{n,\mathbf{k}} |\psi_{n,\mathbf{k}}(\mathbf{r})|^2 \delta(E - E_{n,\mathbf{k}})$, which simulates the STM image, is calculated from the Kohn-Sham (KS) wave functions $\psi_{n,\mathbf{k}}$ and energies $E_{n,\mathbf{k}}$ obtained in the ground state calculation. The spectral function distribution for the $\mathbf{k}$ points along the high symmetry Γ-Σ-Y directions of the original (1×1) Brillouin zone was calculated using a recently proposed method for supercell band structure unfolding [26].

3. Results

3.1. NQR and NMR spectra

Zinc nuclear magnetic resonance was chosen as a sensitive probe of the local zinc environment in the material, and since charge effects are of interest in this work, the principal technique is Zn nuclear quadrupole resonance (NQR). In NQR, one detects transitions between nuclear spin levels split by local electric field gradients, due to a coupling to the nuclear quadrupole moment. Thus NQR provides direct information on local charge distributions. Notably, no external magnetic field is necessary for pure NQR. We have also successfully detected Zn nuclear magnetic resonance in external fields up to 11 T to aid in spectral line identification, but our focus here is on NQR. In the general case of both quadrupolar and magnetic (Zeeman) splitting, the nuclear spin Hamiltonian reads [27]

$$H = -\gamma \mathbf{B}\mathbf{I} + \frac{e^2 Q V_{zz}}{4I(2I-1)} \left[3I_z^2 - I^2 + \eta \left(I_x^2 - I_y^2 \right) \right] \tag{1}$$

where γ is the gyromagnetic ratio of the ^{67}Zn nucleus, $\mathbf{I}$ its spin, Q its quadrupole moment, $\mathbf{B}$ the external magnetic field, V_{xx}, V_{yy} and V_{zz} the principal components of the electric field gradient (EFG) tensor, $\eta = |(V_{xx} - V_{yy})/V_{zz}|$, and $I = 5/2$ for ^{67}Zn. In the case of pure NQR, $\mathbf{B} = 0$ and the analysis of (1) simplifies considerably. When the EFG tensor is axially symmetric ($\eta = 0$), the Hamiltonian gives rise to two NQR lines, corresponding to transitions 1/2→3/2 and 3/2→5/2 with frequencies $\nu_{3/2\to5/2} = 2\nu_{1/2\to3/2}$ (the negative spin levels are degenerate). In the opposite limit of $\eta \approx 1$, the two lines merge into one. YBCO possesses two distinct copper sites — chain Cu and in-plane Cu — which can both in principle be occupied by the substituting Zn. It is well known from previous NMM/NQR studies that $\eta \approx 0$ for in-plane Cu and $\eta \approx 1$ for chain Cu sites. Thus *a priori* one would expect the Zn NQR spectrum

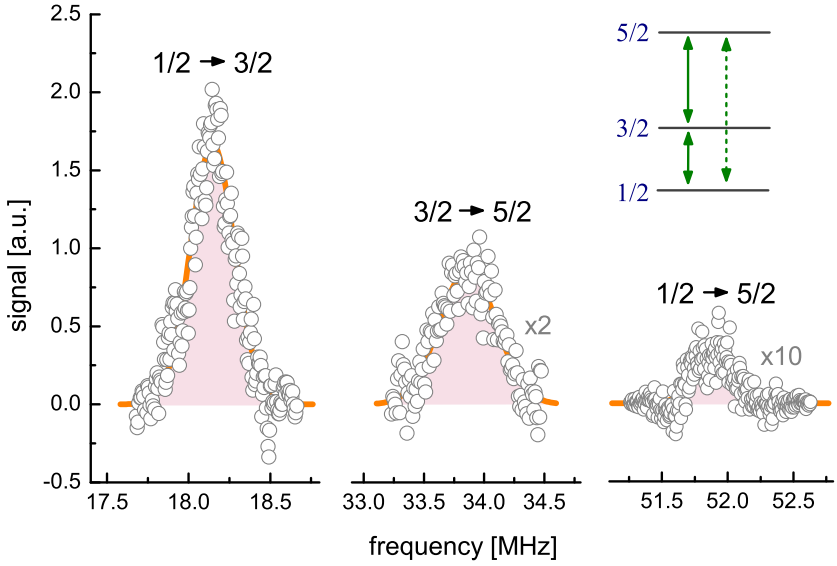

Figure 1. NQR signal of ^{67}Zn (spin 5/2) in YBCO-7, at 80 K. All three possible transitions for spin-5/2 NQR were detected, including the "forbidden" transition 1/2→5/2, showing that the local EFG at the zinc site is not axially symmetric. For clarity, the 3/2→5/2 and 1/2→5/2 intensities have been magnified by a factor of 2 and 10, respectively.

to have two sets of lines, one with $\eta \approx 0$ (i.e. two equally spaced lines) and one with $\eta \approx 1$ (i.e. a single line). Yet in the experiment only one set is observed (Fig. 1), and it clearly breaks axial symmetry: the two strong lines are unequally spaced, and the"forbidden" line corresponding to 1/2→5/2 can be detected. Detection of all three lines in the correct frequency and intensity ratios proves that the signal is due to ^{67}Zn, as there are no other spin-5/2 nuclei in the system.

However, one must still decide whether the observed signal in Fig. 1 originates from chain or in-plane Zn sites. Here an additional NMR experiment with external field is helpful. In an oriented powder, the full Zn NMR Hamiltonian (1) yields a strong central line at $\nu \approx \gamma B$ and two pairs of quadrupolar satellite lines (which are strongly broadened if $\eta > 0$). Two relatively sharp and distinct central lines are observed in Zn NMR at 11 T (Fig. 2a), with the faint signal most likely originating from chain sites. Since Zn chemically prefers to substitute for Cu in the planes, the amount of Zn in the chains is smaller than the nominal 25% of all Zn impurities, and thus the chain signal is more than 5 times weaker than the in-plane Zn NMR. Importantly, no sharp satellite lines are observed, implying that both in-plane and chain Zn have $\eta > 0$. Broadened satellites for $\eta > 0.2$ were not reliably detectable because of great experimental difficulties in Zn NMR. Namely, due to small Zn γ and large Q, the quadrupolar and Zeeman contributions to the NMR signal are comparable at ~ 10 T, making the satellite lines spread out over a large frequency/field range in an oriented powder. NMR in an unoriented powder was attempted in order to see the quadrupolar effects more clearly, but the great spread of the line and uncontrollable partial orientation of the powder in 11 T fields made the results quantitatively unreliable. Yet qualitatively

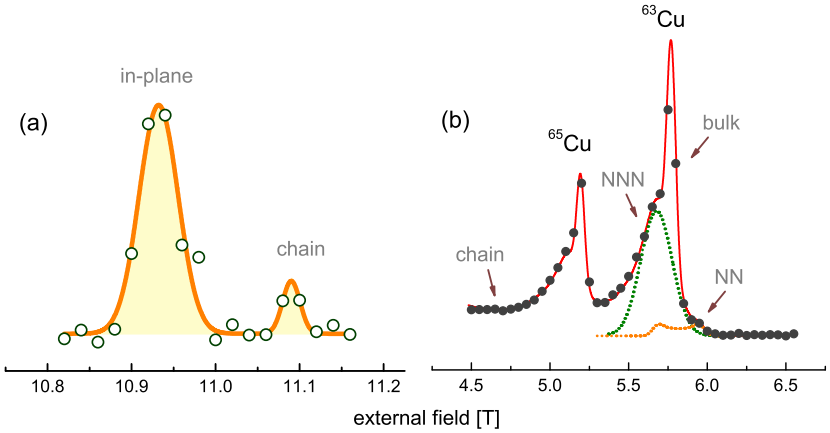

Figure 2. a) Field-sweep measurement of Zn NMR, at a frequency of 29.34 MHz and 70 K. Two lines are visible, with the weaker signal most probably originating from in-chain Zn impurities. Inset: section of Cu NMR field-sweep spectrum measured in an oriented powder at a frequency of 30.46 MHz and at 80 K. b) High-field part of field sweep NMR spectrum of copper in YBCO-Zn. Two contributions other than the bulk line are plotted as dotted lines. The fit was performed consistently on both ^{63}Cu and ^{65}Cu lines, taking into account the different gyromagnetic factors and quadrupolar moments. Due to different symmetry of the nn line ($\eta \approx 0.2$ in the quadrupolar Hamiltonian given in Eq. (1), compared to $\eta \approx 0.03$ for bulk and further neighbour signal) it is partially resolved in NMR, but completely overlapped by the bulk signal in pure NQR. The offset on the low-field side is due to chain Cu.

we are certain that the in-plane signal has η significantly greater than zero, and consistent with $\eta = 0.25$ as seen in pure NQR.

Due to the symmetry of the chain environment, the chain sites must by contrast have η close to one, leading to the conclusion that the NQR lines in Fig. 1 are from in-plane Zn. We emphasize that the difference of $\eta = 0.25$ and $\eta \approx 1$ is very large in terms of the EFG tensor components $V_{\alpha\alpha}$. An extensive search for chain Zn NQR was undertaken from ~ 8.6 MHz up to ~ 45 MHz without results. This implies that the chain NQR signal is either too small to be observed at all, or in the low-frequency range below 8 MHz (as would be expected from a comparison to the equivalent Cu EFG components). The combined arguments of NMR, site symmetry and preferential substitution thus leave no doubt as to the detected NQR originating from in-plane substituted Zn.

The resonance lines barely move with temperature, indicating that the asymmetry is a property of the ground state. Thus all components of the EFG tensor at the zinc site are determined from the ^{67}Zn NQR spectrum alone. Using the known value of Q, we obtain $(V_{zz}, V_{xx}, V_{yy}) = (-50.4, 31.5, 18.9) \cdot 10^{21}$ V/m^2, yielding $\eta = 0.25$. These values are in stark contrast to those at the in-plane Cu sites: the magnitude of V_{zz} at the Zn site is about five times larger than at the bulk Cu site, while the asymmetry at the latter is only $\eta \approx 0.03$. Therefore the small intrinsic orthorhombicity of YBCO [28], related to the appearance of CuO chains, cannot be the cause of the large NQR asymmetry observed at the Zn site — if it were, one would expect a similar

D_4 symmetry breaking at the planar Cu sites as well. We conclude that Zn substitution causes a large local lattice distortion. Also, the charge environments of the Zn and bulk plane Cu sites are obviously very different. Previous cluster calculations [23, 29] found that the net charge at the Zn site was indeed larger than on a bulk copper site, without considering lattice distortions.

In addition to Zn NQR/NMR, copper sites in the neighbourhood of the Zn impurities are of interest, providing insight into the range of electronic effects at the Zn site itself. We have performed field-sweep Cu NMR to identify the nearest-neighbour (nn) signal and separate it from other further-neighbour contributions. The relevant part of the field-sweep spectrum is shown in Fig. 2b. The two sharp peaks are bulk ^{65}Cu and ^{63}Cu quadrupolar satellites; central lines are not shown for clarity. The positions of the bulk peaks agree precisely with pure NQR of the unsubstituted compound, and with previous measurements. Qualitatively, four distinct contributions can be glimpsed in the spectrum, which were taken to be due to chain Cu (offset on low-field side), bulk in-plane Cu (sharp peaks), further Zn neighbour Cu (shoulder on low-field side of bulk Cu line) and nearest-neighbour Cu (shoulder on high-field side of the bulk signal). The contributions were quantitatively separated using the following assumptions and constraints: simultaneous treatment of both Cu isotopes, with known intensity, gyromagnetic factor and quadrupolar moment ratios; known quadrupolar coupling constants for bulk, further Zn neighbour and chain Cu sites from NQR; $\eta > 0$ for the nearest-neighbour signal (since it is not resolved in pure NQR, implying a ν_Q similar to the bulk site). Bulk and further neighbour lines were modeled as symmetric Gaussian shapes, while nn and chain contributions were calculated from an exact diagonalization of the NMR Hamiltonian (1) with spin 3/2. and oriented powder averaging. The asymmetry of the nn Cu line turns out to be $\eta \approx 0.2$, and its ν_Q within 1% of the bulk Cu value. Thus the bulk and nn Cu lines completely overlap in pure NQR, while they are partially resolved in the NMR spectrum. To our knowledge this is the first observation of the true nn line, since in previous work [19, 30] the nnn signal (shoulder to the left of the bulk peak in Fig. 2b, appears the same in pure NQR) was taken to be from nn Cu on account of intensity ratios. The finite η at the nn Cu site arises, as expected from Zn NQR, due to the lattice distortion brought upon by Zn.

3.2. Spin-lattice relaxation rates

Temperature-dependent spin-lattice relaxation measurements on ^{67}Zn provide further evidence of the peculiar electronic surroundings of the Zn impurity. The first important observation is that the Zn relaxation is slow, and involves a two-step process at temperatures below $\sim$ 200 K (Fig. 3a). Although the data also allow a stretched-exponential fit, which would indicate local disorder as e.g. in CDW systems [32, 33], we can rule that out: even a small amount of disorder broadens the NQR line significantly (in our sample 3% of Zn broadens the bulk-Cu NQR line by a factor $\sim$ 5.) Yet the relative width of the Zn lines in Fig. 1 is barely larger than the width of the Cu NQR line in the *unsubstituted* material, implying that the local environments of the in-plane Zn impurities are uniform. This is corroborated by the sharp onset of Meissner effect. Conversely, if some Zn atoms did have different environments, their NQR lines would be strongly shifted and thus undetectable in the present measurement. We conclude that the two-step relaxation is an intrinsic property of every single Zn site, and quantify it by a simple model. The Zn nuclear moments are insulated from

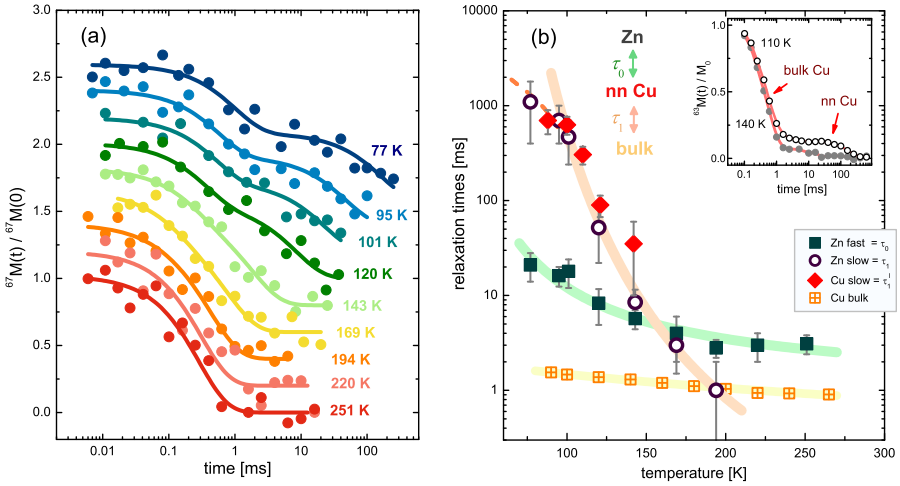

Figure 3. a) ^{67}Zn spin-lattice relaxation curves for all measured temperatures, with two-component relaxation fits, Eq. 3. The curves are offset for clarity in steps of 0.2, with the highest-temperature measurement unshifted. The different temperature dependences of the fast and slow relaxation components are clearly visible. b) Spin-lattice relaxation times of the ^{67}Zn NQR 1/2→3/2 transition, nn and bulk ^{63}Cu NQR, in dependence on temperature. Two components of the Zn relaxation are plotted (full squares and empty circles), obtained from a double relaxation model (see text). Thick full lines are Arrhenius fits for the primary and secondary relaxation. The thin dashed line is a proposed two-phonon process correction for the secondary relaxation (see text). The slow copper relaxation process (full diamonds) is seen to follow the slow Zn relaxation. Bulk Cu relaxation (crossed squares) is significantly faster than all others and follows a "nearly AF" temperature dependence [line, Eq. (4)]. Pure Curie-Weiss behaviour would be a horizontal line. All raw relaxation times are rescaled to the standard definition of T_1 with the appropriate phase-space factors [31]: 10 for ^{67}Zn and 3 for ^{63}Cu. Inset: spin-lattice relaxation measurements of copper NQR at 31.5 MHz, which also contain a slow process at low temperatures. The large, quickly decaying contribution is of bulk copper.

the planar metal, and feed exclusively a *local* magnetization reservoir — which we will show is consistent with localized electronic states — with an "internal" rate $1/\tau_0$. The local states are assumed to equilibrate quickly with nn Cu nuclear moments, which in turn relax slowly to the wider environment with an "external" rate $1/\tau_1$ (schematic on Fig. 3). The magnetizations ^{67}M and ^{63}M of the Zn and nn Cu moments then evolve according to

$$\begin{aligned} \frac{d^{67}M}{dt} &= -\frac{1}{\tau_0}\left(^{67}M - {}^{63}M\right) \\ \frac{d^{63}M}{dt} &= -\frac{1}{\tau_1}{}^{63}M - \frac{1}{\tau_0}\left(^{63}M - {}^{67}M\right). \end{aligned} \tag{2}$$

Solving the coupled system gives the ^{67}Zn magnetization,

$$\frac{^{67}M(t)}{^{67}M_0} = A_+ e^{-\alpha_+ t} + A_- e^{-\alpha_- t}. \tag{3}$$

with $\alpha_\pm = 1/\tau_0 + 1/2\tau_1 \pm \sqrt{1/\tau_0^2 + 1/4\tau_1^2}$ and $A_\pm = \frac{1}{2}\left(1 \mp 1/\sqrt{1 + 4\tau_1^2/\tau_0^2}\right)$. Such a coupled double-exponential relaxation fits the experimental curves well (inset to Fig. 3), up to $T \approx 200$ K where τ_1 becomes too small to be resolved. The constants $A_\pm$ are wholly given in terms of the two relaxation times τ_0 and τ_1, without introducing additional fitting parameters. The fit thus has the same number of parameters as a stretched exponential, and yields smaller overall least-square deviations than stretched-exponential fits at low temperatures. A somewhat similar relaxation model was proposed for nn Cu in Zn-Y248 [30].

Additional corroboration of the two-step relaxation model can be obtained from nn Cu spin-lattice relaxation measurements. The nn Cu signal was identified with the help of field-sweep NMR, as explained in detail above. Unfortunately, the nn Cu and bulk Cu lines overlap in pure NQR; this is also perhaps the reason why the true nn signal was overlooked in previous work, with the next-nearest neighbors possibly being confused with the nearest ones [19, 30]. Nevertheless, a long tail due to nn Cu was detected in the NQR relaxation curves (Fig. 3b inset), with the values of the relaxation times τ_1' agreeing with τ_1 from Zn measurements.

The finding of a slow nn Cu relaxation in agreement with the slow Zn process and the large difference between τ_0 and τ_1 at low temepratures constrain our interpretation by excluding several simple alternatives. The second, 'external' process has to be the slower one, or the two stages would not be resolved. The first magnetization reservoir has to feed the second exclusively, otherwise the specific algebraic relationships $2\alpha_- \approx 1/\tau_1$ and $\alpha_+ \approx 2/\tau_0$, valid when $\tau_0 \ll \tau_1$, would change and spoil the rescaling of raw data, required for the extracted Zn $\tau_1(T)$ to coincide with the directly measured Cu $\tau_1'(T)$. Finally, the intermediate states, by which Zn moments relax to the nn Cu moments, do not thermalize, or otherwise a third magnetization reservoir would be necessary to describe the data. In the limit of long $\tau_1 \gg \tau_0$, $A_\pm \to 1/2$, in agreement with the experimental relaxation curves shown in Fig. 3a. This agreement eliminates a three-step process.

The relaxation times τ_0, τ_1 and τ_1' are plotted in Fig. 3b, with clearly very different magnitude and temperature behaviour. Bulk Cu relaxation (which agrees with measurements in unsubstituted YBCO [34]) is shown for comparison, and it is qualitatively different than Zn in the entire temperature range, in addition to being significantly faster. This shows that the electronic fluctuations to which the Zn impurity is exposed are not metallic, as for the bulk copper sites. A quantitative analysis and comparison to electronic structure calculations will make this statement more precise, and elucidate the nature of the fluctuations.

4. Analysis and discussion

4.1. NQR relaxation

Apart from the two-step relaxation process, the Zn τ_0 and τ_1 data are irreconcilable with a metallic environment, either the usual (Korringa) $1/(T_1T) \sim$ *const.*, or the "nearly AF" temperature dependence [35, 36, 37]

$$1/(T_1T) \sim a + b/(T + T_{AF}), \tag{4}$$

obeyed by the bulk copper T_1 in Fig. 3b. Also, previous observations of enhanced relaxation rates and NMR shift at further neighbor copper sites [19] and lithium impurities [38, 39], interpreted in terms of strong nearly-AF metallic fluctuations,

are in stark contrast to the observed low-temperature slowing down of Zn relaxation. Therefore the immediate Zn environment is insulating, rather than a nearly-AF metal. In line with that reasoning, the temperature dependence of the slow component τ_1 is well described by an Arrhenius curve of the form $1/\tau_1 \sim e^{-\Delta/kT}$ with a gap of $\Delta \sim 0.1$ eV, consistent with a superexchange interaction between the nn Cu electronic local moments. The activated behavior implies that the cluster is insulating, while the scale of the interaction confirms the conjecture [2] that the cluster around the Zn site is AF, supporting the original explanation for the observed AF Curie law [2]. The insulating cluster is evidently small enough for AF fluctuations to appear as a finite-size effect, as seen in molecular magnets [40]. Such collective fluctuations are expected to enhance the Curie response over that of individual spins.

As a fine detail, the τ_1 data points in Fig. 3 seem to deviate from the Arrhenius curve at lowest temperatures and longest relaxation times. Although we have only one τ_1 and one τ_1' point there, the tendency of both to the same deviation brings us to tentatively propose a correction at the lowest temperatures, shown by a dashed line in the figure. It was modelled by the dominant two-phonon Raman process [27], with the characteristic temperature dependence $1/T_1 \sim T^2$ (which might actually be faster due to the relevant temperatures being close to the Debye temperature). It is not unrealistic that the transition matrix elements are small enough to lead to relaxation times of the order of 0.1 second [27]. However, the small number of data points, at the edge of the measurable range, precludes a positive identification.

The fast Zn relaxation component, τ_0, corresponding to the 'internal' relaxation process, is similarly satisfactorily described by an activated temperature dependence, albeit with a much smaller gap than τ_1. A fit (solid line through τ_0 points in Fig. 3b) yields a gap of ~ 20 meV, suggesting that slightly gapped local electronic states are responsible for the relaxation. Cluster and periodic DFT calculations indicate that just such states arise induced by Zn, and are responsible for the local D_4 symmetry breaking, as follows.

4.2. Microscopic analysis

The Zn 3d orbital is closed ($3d^{10}$), making it a good candidate for local DFT calculations without strong correlations [23, 29]. We have performed a cluster DFT calculation of molecular states in plaquettes of four Cu atoms, a central Zn impurity, and their oxygen pyramids [21, 22, 41], shown in Fig 4a. We obtain a lattice distortion with broken tetragonal symmetry, with low-lying excited states appearing with the distortion. The D_4 symmetry is lost by breaking the degeneracy between the two oxygens in the planar unit cell (Fig. 4b). The same symmetry breaking appears in the LTT tilt [1, 42]. The excited states are ≈ 100 meV above the ground state, which is an overestimate, given the crudeness of the calculation.

We also performed periodic DFT calculations [24, 25, 26] with supercells consisting of 3×3 and 5×5 La_2CuO_4 unit cells, with central Cu replaced by Zn. We intentionally employ the tendency of DFT calculations to spurious metallicity, so as to model the disruption by Zn under circumstances least favorable to it. Remarkably, Zn breaks the *electronic* D_4 symmetry in this ordered lattice even if the atoms are held fixed in their ideal-lattice positions, as shown in Fig. 5a. (In STM measurements [43] the symmetry is broken even further, which may be a surface effect.) Breaking the degeneracy of the two oxygens in the unit cell splits the van Hove singularity [42]. For realistic 4% Zn doping the excitation scale from E_f drops to about 20 meV (Fig. 5b),

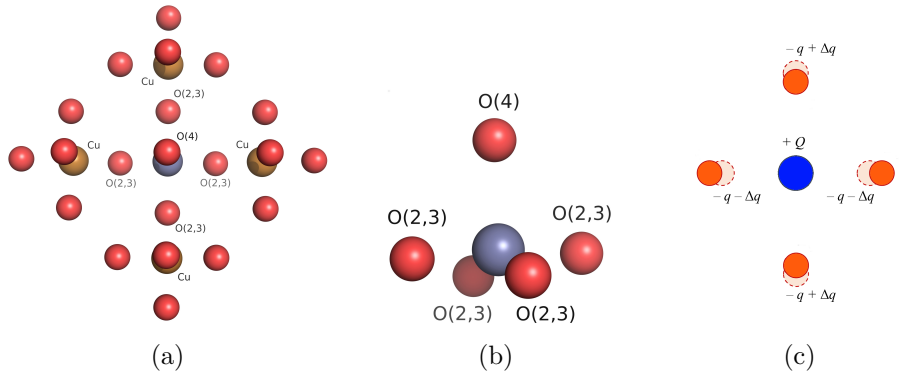

Figure 4. (a) The entire DFT cluster (without point charges) used for electronic structure calculations in ORCA. O(4) are apical, and O(2,3) in-plane oxygen atoms, and the grey central atom is zinc. Realistic YBCO lattice parameters are taken from X-ray diffraction. (b) Deformation of the ZnO_5 pyramid. The two $O_{2,3}$ oxygens in the planar unit cell are no longer equivalent. (c) Illustration of the simple 2D electrostatic argument used in the text. The movement of ions is denoted by the dotted outlines. Here $Q = 4q$.

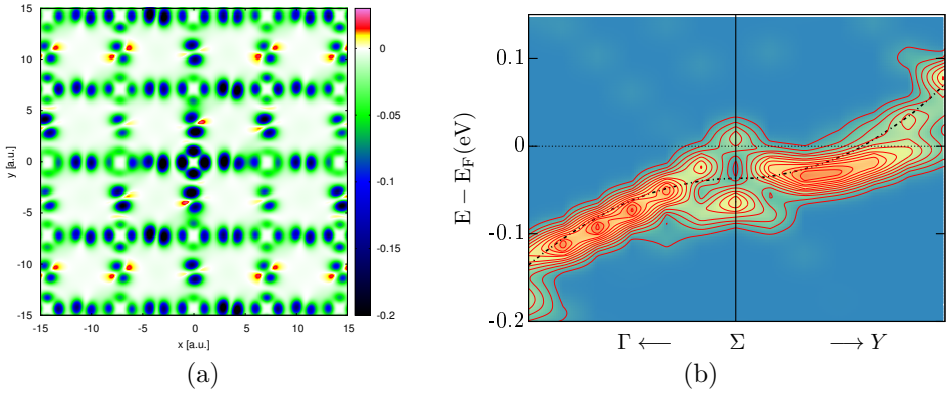

Figure 5. (a) Difference of simulated STM images, integrated in a 20 meV window at E_f, for a slab with 3×3 supercell of La_2CuO_4 unit cells with and without the central Cu replaced by Zn. Note the different densities in the x- and y-directions. Color scale units: $10^{-3}a_0^{-3}$. (b) Spectral function (arbitrary units) near the van Hove singularity for a 5×5 supercell, corresponding to 4% Zn doping in the plane.

which is an underestimate, because of the artificial periodicity and lack of atomic relaxation in the model system.

Qualitatively, the electronic D_4 symmetry breaking in the periodic calculation is consistent with the deformation in the small-cluster calculation. The energy scale of the local cluster is bracketed between 20 and 100 meV by these two limits. Without discussing the coupling mechanism, we conclude that the Zn moments relax to nn Cu moments via electronic states of the planar ZnO_4 cluster.

The D_4 symmetry breaking may be understood intuitively as a simple electrostatic effect. In a first approximation, the ions in the basic ZnO_4 square can be regarded as point charges (Fig. 4c). The square is then unstable in two ways. First, a transfer

of a small charge Δq between the oxygens and simultaneous shift of the ions *in the plane* (pictured in Fig. 4c) lowers the energy and breaks the square symmetry. The tendency towards such a transfer is corroborated by the calculation in Fig. 5a, which shows an electronic instability ($\Delta q \neq 0$) in the plane when the atoms are *not* allowed to relax, and oxygen orbitals must accommodate the extra charge $\pm\Delta q$. Second, even if $\Delta q = 0$, the square is still unstable towards a shift of the oxygens *out of the plane*, with one oxygen in the unit cell going up, and the other down. This instability becomes relevant when all Zn and O orbitals are closed — as they are in the present case — making charge transfer impossible. Such a shift in itself keeps the mirror symmetry of the plane intact, but once the apical oxygen (and other ions) are included, the mirror symmetry is broken and the lowest energy state is reached by oxygens shifting unequally both out of the plane and towards/away from the Zn. This is seen in the full relaxed 3D cluster calculation, Fig. 4b. Importantly, because the Zn impurity is highly charged in comparison to its surroundings, long-range contributions from far-away ions cannot remove the Coulomb instability as they do in the bulk; similarly, entropy contributions to the free energy are not important for the local effects of Zn. Also, closed Zn and O orbitals mean that the point-charge approximation is expected to be quite good. We conclude that the D_4 symmetry breaking occurs because the Zn impurity triggers elementary electrostatic instabilities in a local point-charge (closed-orbital) configuration.

Our observation that the Zn cluster is insulating is in accord with the observation of a zero-bias peak at the Zn site in STM [5]. We concur with Ref. [5] that the peak is a scattering resonance, i.e. interference peak in the Friedel screening. An interference maximum is not surprising at an insulating site, like at the position of a hole in an antenna array. For Zn-BSCCO, this picture has been corroborated by a concrete calculation [44]. The question is how big the insulating hole is, and we find that it includes the nn coppers, where STM [5] finds zero DOS. As also noted in Ref. [5], the appearance of metallic screening at zero bias is direct evidence that SC is destroyed around the Zn site, because the STM measurements were carried out deep below T_c.

4.3. Inferences for collective states

The present results have important repercussions for the composition of the SC metal in the cuprates. The gapped NQR relaxation of the Zn and nn Cu sites, and the large EFG's at the Zn site, are incompatible with a metallic environment. However, an insulating environment indicates that the in-plane oxygen atoms in the SC materials are in a different orbital configuration than in the parent materials [6]. One can express the ionic doping proposal [7] as a chemical reaction in the solid state,

$$Cu^{2+} + O^{2-} \rightleftharpoons Cu^{+} + O^{-}, \tag{5}$$

whose balance is tuned by doping. As mentioned above, the right-hand-side ionic configuration was observed very early [8] to appear concomitantly with SC. We observe the insulating islands precisely where the O $2p^5$ (O^-) configuration of the SC metal *cannot* appear, because Zn is already in the $3d^{10}$ (Zn^{2+}) configuration next to the parent $2p^6$ (O^{2-}). The islands are in the original (parent) AF Mott insulator configuration. Because the parent $3d^9$ (Cu^{2+}) configuration is converted to $3d^{10}$ (Cu^+) in the SC compositions, the on-site repulsion U_d, due to the large ionization energy of the $3d^8$ (Cu^{3+}) configuration, is a second-order effect in the normal state of the SC metal at low energy. Indeed, a careful dynamical treatment of U_d in the limit of

significant Cu–O covalency, but starting from the $3d^{10}$ vacuum, shows that the direct effects of U_d are observed in ARPES away from the Fermi energy [45].

As described so far, the observed local reversal of the reaction (5) to the left-hand-side would reduce the SC fraction, but not necessarily the SC T_c. However, we have uncovered an additional unsuspected effect of the Zn impurities on the SC metal itself. The Coulomb domino effect around Zn sites breaks D_4 symmetry and lifts the degeneracy of the oxygens in the planes, in the same manner as the LTT tilt in LBCO [1, 42]. In Fig. 5a, it progresses to the next-nn O sites beyond the nn Cu sites (consistently with the fact that the nn Cu sites are not metallic either), involving by extension the next-nn Cu sites on their other side. This observation elevates the O_x–O_y site-energy splitting to a universal antagonist of SC in the cuprates. Its microscopic effect on the SC is obscured in the LTT tilt, because the split van Hove singularity shifts electrons away from the Fermi surface [42]. Any lowering of the density of states at the Fermi surface should lower T_c, whatever the SC mechanism. We find, however, that scattering on the oxygen-splitting phonon is negatively affecting the SC electrons *microscopically* in all cuprates, given that all are subject to the Zn effect.

The requirement that the two oxygens in the unit cell be degenerate is a qualitative constraint on the SC mechanism. It means that the oxygen orbitals in the superconducting metal must appear in symmetry-determined, not parameter-determined, superpositions, because only the former are singularly perturbed by even a small O_x–O_y splitting. One such oxygen singlet superposition was found [46] to destabilize the Zhang-Rice singlet [12], provided the Cu–O overlap is effectively reduced in favor of the O_x–O_y overlap. Such a reduction appears both in the standard slave-particle scenarios starting from the $3d^9$ vacuum [9], and if $3d^{10}$ is the relevant vacuum [45], as inferred here.

As an additionial point, our measurements suggest an explanation of the effects of Zn doping on the LTT phase in LBCO [47]. The charge-stripe correlations disappear because they are disrupted by the insulating islands. The spin-stripe response is enhanced because the LTT tilt is stabilized by the similarly-acting Zn. Like in the local Curie response induced by the same Zn, magnetic responses are again enhanced by the non-magnetic Zn impurity because it acts strongly in the charge channel — creating an insulator, and deforming the lattice, respectively.

5. Conclusion

We have measured the NQR signal in Zn-substituted optimally doped YBCO on the Zn sites themselves for the first time. We find that Zn creates large insulating islands. Instead of the metal shielding the Zn impurity, the impurity reverses the metallic vacuum, so that the metal disappears. Locally, the optimally doped material reverts to the closed O $2p^6$ orbitals characteristic of the parent compound, in which the Cu $3d^9$ orbitals are open, and magnetic. Conversely, the SC metal vacuum is based on open O $2p^5$ orbitals and closed Cu $3d^{10}$ orbitals. Zn impurities are experimentally observed to break the D_4 symmetry of the lattice site which they occupy. Calculations show this occurs by breaking the degeneracy of the two planar oxygen orbitals within a unit cell, which is thus found to be strongly detrimental to SC in all cuprates, pointing to the direct involvement of O_x–O_y degenerate superpositions in the SC mechanism.

6. Acknowledgments

Conversations with S. Barišić, A. Dulčić, P. Lazić, S. Mazumdar, and D. Pavuna are gratefully acknowledged, as well as the help of T. Cvitanić with sample preparation. D.K.S. thanks the organizers for an invitation and a stimulating time at the ECRYS-2011 Workshop on Electronic Crystals.

This work was supported by the Croatian Government under project No. 119-1191458-0512, by the University of Zagreb grant No. 202301-202353, and by the Croatian Science Foundation (HRZZ) Grant 2729.

References

[1] Axe J D, Moudden A H, Hohlwein D, Cox D E, Mohanty K M, Moodenbaugh A R and Xu Y 1989 *Phys. Rev. Lett.* **62**(23) 2751–2754
[2] Mahajan A, Alloul H, Collin G and Marucco J 2000 *The European Physical Journal B - Condensed Matter and Complex Systems* **13** 457–475
[3] Mila F and Rice T 1989 *Physica C: Superconductivity* **157** 561 – 570
[4] Terashima K, Sato T, Nakayama K, Arakane T, Takahashi T, Kofu M and Hirota K 2008 *Phys. Rev. B* **77**(9) 092501
[5] Pan S H, Hudson E W, Lang K M, Eisaki H, Uchida S and Davis J C 2000 *Nature* **403** 746–750
[6] Barlingay C, García-Vázquez V, Falco C M, Mazumdar S and Risbud S H 1990 *Phys. Rev. B* **41**(7) 4797–4800
[7] Mazumdar S 1989 A unified theoretical approach to superconductors with strong Coulomb correlations: the organics, $LiTi_2O_4$, electron- and hole-doped copper oxides and doped $BaBiO_3$ *Interacting electrons in reduced dimensions* ed Baeriswyl D and Campbell D K (Plenum Press, New York) pp 315–329
[8] Bianconi A, Castellano A, Santis M D, Rudolf P, Lagarde P, Flank A and Marcelli A 1987 *Solid State Communications* **63** 1009 – 1013
[9] Qimiao Si, Yuyao Zha, Levin K and Lu J P 1993 *Phys. Rev. B* **47** 9055–76
[10] Emery V J 1987 *Phys. Rev. Lett.* **58** 2794–7
[11] Pavarini E, Dasgupta I, Saha-Dasgupta T, Jepsen O and Andersen O K 2001 *Phys. Rev. Lett.* **87**(4) 047003
[12] Zhang F C and Rice T M 1988 *Phys. Rev. B* **37** 3759–61
[13] Sunko D K and Barišić S 2007 *Phys. Rev. B* **75**(6) 060506
[14] Perry J K, Tahir-Kheli J and Goddard W A 2002 *Phys. Rev. B* **65**(14) 144501
[15] Lee K H and Hoffmann R 2006 *The Journal of Physical Chemistry A* **110** 609–617
[16] Božin E S and Billinge S J L 2005 *Phys. Rev. B* **72**(17) 174427
[17] Tahir-Kheli J and Goddard W A 2011 *The Journal of Physical Chemistry Letters* **2** 2326–2330
[18] Adachi S, Kasai C, Tajima S, Tanabe K, Fujihara S and Kimura T 2001 *Physica C: Superconductivity* **351** 323 – 328 ISSN 0921-4534
[19] Itoh Y, Machi T, Kasai C, Adachi S, Watanabe N, Koshizuka N and Murakami M 2003 *Phys. Rev. B* **67**(6) 064516
[20] Mazumder S, Rajagopal H, Sequeira A, Singh J, Rajarajan A K, Gupta L C and Vijayaraghavan R 1989 *Phase Transitions* **19** 97–105
[21] Schäfer A, Horn H and Ahlrichs R 1992 *The Journal of Chemical Physics* **97** 2571–2577
[22] Neese F, Wennmohs F, Hansen A and Becker U 2009 *Chemical Physics* **356** 98 – 109
[23] Bersier C, Renold S, Stoll E P and Meier P F 2005 *Phys. Rev. B* **72**(22) 224514
[24] Giannozzi P, Baroni S, Bonini N, Calandra M, Car R, Cavazzoni C, Ceresoli D, Chiarotti G L, Cococcioni M, Dabo I, Corso A D, de Gironcoli S, Fabris S, Fratesi G, Gebauer R, Gerstmann U, Gougoussis C, Kokalj A, Lazzeri M, Martin-Samos L, Marzari N, Mauri F, Mazzarello R, Paolini S, Pasquarello A, Paulatto L, Sbraccia C, Scandolo S, Sclauzero G, Seitsonen A P, Smogunov A, Umari P and Wentzcovitch R M 2009 *Journal of Physics: Condensed Matter* **21** 395502
[25] Perdew J P, Burke K and Ernzerhof M 1996 *Phys. Rev. Lett.* **77**(18) 3865–3868
[26] Popescu V and Zunger A 2012 *Phys. Rev. B* **85**(8) 085201
[27] Abragam A 1983 *Principles of Nuclear Magnetism (International Series of Monographs on Physics)* (Oxford University Press)
[28] Pennington C H, Durand D J, Slichter C P, Rice J P, Bukowski E D and Ginsberg D M 1989 *Phys. Rev. B* **39**(4) 2902–2905

[29] Kaplan I G, Soullard J and Hernández-Cobos J 2002 *Phys. Rev. B* **65**(21) 214509
[30] Williams G V M and Krämer S 2001 *Phys. Rev. B* **64**(10) 104506
[31] Walstedt R E 2008 *The NMR Probe of High-Tc Materials* (Springer)
[32] Dubson M A and Holcomb D F 1986 *Phys. Rev. B* **34**(1) 25–35
[33] Phillips J C 1996 *Reports on Progress in Physics* **59** 1133
[34] Uldry A and Meier P F 2005 *Phys. Rev. B* **72**(9) 094508
[35] Moriya T, Takahashi Y and Ueda K 1990 *Journal of the Physical Society of Japan* **59** 2905–2915
[36] Monien H, Pines D and Takigawa M 1991 *Phys. Rev. B* **43**(1) 258–274
[37] Nakai Y, Iye T, Kitagawa S, Ishida K, Ikeda H, Kasahara S, Shishido H, Shibauchi T, Matsuda Y and Terashima T 2010 *Phys. Rev. Lett.* **105**(10) 107003
[38] Bobroff J, MacFarlane W A, Alloul H, Mendels P, Blanchard N, Collin G and Marucco J F 1999 *Phys. Rev. Lett.* **83**(21) 4381–4384
[39] Ouazi S, Bobroff J, Alloul H and MacFarlane W A 2004 *Phys. Rev. B* **70**(10) 104515
[40] Wang Z, Datta S, Papatriantafyllopoulou C, Christou G, Dalal N S, van Tol J and Hill S 2011 *Polyhedron* **30** 3193 – 3196
[41] Neese F 2012 *Wiley Interdisciplinary Reviews: Computational Molecular Science* **2** 73–78
[42] Barišić S and Zelenko J 1990 *Solid State Communications* **74** 367–370
[43] Hamidian M H, Firmo I A, Fujita K, Mukhopadhyay S, Orenstein J W, Eisaki H, Uchida S, Lawler M J, Kim E A and Davis J C 2012 *New Journal of Physics* **14** 053017
[44] Wang L L, Hirschfeld P J and Cheng H P 2005 *Phys. Rev. B* **72**(22) 224516
[45] Barišić O S and Barišić S 2012 *J. Supercond. Nov. Magn.* **25**(3) 669–676
[46] Sunko D K 2009 *Journal of Experimental and Theoretical Physics* **109** 652–658
[47] Hücker M, Zimmermann M, Xu Z, Wen J, Gu G, Tian W, Zarestky J and Tranquada J 2011 *Journal of Superconductivity and Novel Magnetism* **24**(3) 1229–1233